First posted online on 11 May 2018 as 10.1242/dev.160739
Access the most recent version at http://dev.biologists.org/lookup/doi/10.1242/dev.160739

Nppa and Nppb act redundantly during zebrafish cardiac development to confine AVC marker expression and reduce cardiac jelly volume

Daniela R. Grassini, Anne K. Lagendijk, Jessica E. De Angelis, Jason Da Silva, Angela Jeanes, Nicole Zettler, Neil I. Bower, Benjamin M. Hogan & Kelly A. Smith *.

Affiliations:

[1] Institute for Molecular Bioscience, The University of Queensland, Brisbane, Queensland 4072, Australia.

Contact:

k.smith@imb.uq.edu.au

Additional footnotes:

* Corresponding author

© 2018. Published by The Company of Biologists Ltd.

Development • Accepted manuscript

SUMMARY STATEMENT

Nppa and Nppb are mechanoresponsive peptides expressed during cardiomyocyte stress. Double *nppa/nppb* mutant embryos have increased cardiac jelly due to ectopic activation of the atrioventricular canal gene program into the atrium.

ABSTRACT

Atrial natriuretic peptide (*nppa/anf*) and *brain natriuretic peptide* (*nppb/bnp*) form a gene cluster with expression in the chambers of the developing heart. Despite restricted expression, a function in cardiac development has not been demonstrated by mutant analysis. This is attributed to functional redundancy however their genomic location *in cis* has impeded formal analysis. Using genome-editing, we generated mutants for *nppa* and *nppb* and found single mutants indistinguishable from wildtype whereas *nppa*/*nppb* double mutants display heart morphogenesis defects and pericardial oedema. Analysis of atrioventricular canal (AVC) markers show expansion of *bmp4*, *tbx2b, has2* and *versican* expression into the atrium of double mutants. This expanded expression correlates with increased extracellular matrix in the atrium. Using a biosensor for Hyaluronic acid to measure the cardiac jelly (cardiac extracellular matrix), we confirm cardiac jelly expansion in *nppa*/*nppb* double mutants. Finally, *bmp4* knockdown rescues the expansion of *has2* expression and cardiac jelly in double mutants. This definitively shows that *nppa* and *nppb* function redundantly during cardiac development to restrict gene expression to the AVC, preventing excessive cardiac jelly synthesis in the atrial chamber.

Development • Accepted manuscript

INTRODUCTION

At early stages of development (24-30 hours post fertilization [hpf] in the zebrafish), the heart is a double-layered linear tube, with an inner layer of endothelium (called the endocardium) and an outer muscular layer called the myocardium. During cardiac morphogenesis in both zebrafish and mice, the prospective atrial and ventricular chambers of the heart "balloon" out of the heart tube, becoming morphologically and genetically distinct from the atrioventricular canal (AVC). The AVC is a specialized region of the developing heart that partitions the two chambers. It is characterized by *Bmp2/4* (Keyes et al., 2003; Ma et al., 2005; Walsh and Stainier, 2001) and *Tbx2* (Chi et al., 2008; Christoffels et al., 2004; Harrelson et al., 2004) gene expression in the myocardium and *Has2* gene expression in the endocardium (Tien and Spicer, 2005). *Has2* encodes a synthetic enzyme of the extracellular matrix component, Hyaluronic acid (HA), and, congruent with its expression, localized swellings of extracellular matrix (ECM; known as "cardiac jelly") are observed at the AVC. These swellings are the endocardial cushions; primitive structures that will later remodel to form cardiac valve leaflets.

The hierarchical relation between *Bmp2/4* and *Tbx2* has been extensively described, both in fish and mammals. *Bmp2/4* and *Tbx2* depletion share the phenotype of impaired AV boundary establishment (Chi et al., 2008; Harrelson et al., 2004; Ma et al., 2005) and reduced Bmp signaling results in undetectable expression of *Tbx2* in the AVC myocardium, placing Bmp signaling upstream of *Tbx2* (Ma et al., 2005; Shirai et al., 2009; Verhoeven et al., 2011). The zebrafish *jekyll* mutant, which harbours a mutation in the *UDP-Glucose 6-Dehydrogenase* gene (another enzyme of the HA biosynthetic pathway), and *Has2* null mice show a key function for the cardiac jelly in determining both correct patterning and early localised growth of the endocardial cushions (Camenisch et al., 2000; Walsh and Stainier, 2001).

Whilst *Bmp2/4* and *Tbx2* are restricted to the AVC, *Nppa* (also known as ANF; atrial natriuretic factor) and *Nppb* (also known as BNP; brain natriuretic peptide) represent their chamber myocardium counterpart: *Nppa* and *Nppb* expression are enriched in the ballooning surfaces of the cardiac tube and *Nppa* is actively excluded from the AVC by the repressive function of *Tbx2* (Becker et al., 2014; Christoffels et al., 2004; Habets et al., 2002). Despite their compelling expression patterns, little is reported about the function of *Nppa* and *Nppb* during heart development. Null mice for either *Nppa* or *Nppb* lack any obvious

Development • Accepted manuscript

developmental phenotype (John et al., 1995; Tamura et al., 2000). *Nppa* and *Nppb* lie in a conserved gene cluster (Inoue et al., 2003; Tamura et al., 1996) with common regulatory regions that become activated during development (Sergeeva et al., 2016). This co-regulation, their homology and the absence of developmental phenotypes observed in single gene loss-of-function has led to the hypothesis that these two genes are functionally redundant.

Here, we describe the generation of single and double *nppa* and *nppb* zebrafish mutants, now possible with genome-editing methodologies. Consistent with previous reports, single mutants exhibit no overt developmental phenotype. In contrast, double mutants exhibit pericardial oedema, expanded AVC markers and thickening of the cardiac jelly in the atrium of the early embryonic heart. These data support the notion that *nppa* and *nppb* function redundantly and demonstrate that *nppa/nppb* double mutants play a previously unappreciated role in cardiac development by restricting AVC gene expression and repressing ECM accumulation in the atrial chamber.

RESULTS AND DISCUSSION

nppa and *nppb* act redundantly during early cardiac morphogenesis

In zebrafish, the *nppa* and *nppb* loci reside in a gene cluster on chromosome 8, separated by approximately 2.5Kb (Fig. 1A). This proximity precludes a classical strategy of generating double homozygous mutants by homologous recombination. To overcome this, we undertook sequential mutagenesis of the two loci, first generating an *nppa* mutant line utilising TALEN technology, and then targeting the *nppb* locus in the *nppa* mutant background using the CRISPR/Cas9 system. Simultaneously, *nppb* single mutants were created. For *nppa*, exon 1 was targeted producing a 4 base pair (bp) deletion at 55 bp of the coding region ($nppa^{uq19ks}$). This results in normal protein sequence until amino acid 18, followed by frame-shifted sequence to amino acid 23 and then translational termination (Fig. 1A,B), preventing generation of the 139 amino acid wild type protein. For *nppb*, exon 2 was targeted and two alleles were generated. The mutant locus $nppb^{uq20ks}$, linked *in cis* to the $nppa^{uq19ks}$ allele, carries a 39 bp insertion containing a stop codon, resulting in a shorter protein at 80 amino acids long (Fig. 1A,B; full-length wildtype protein is 129 amino acids long). The single $nppb^{uq21ks}$ mutant allele harbours a 10 bp frameshift insertion at amino acid 80, encoding 15 out-of-frame amino acids until termination at 95 amino acids in length (Fig. 1A,B). In all three instances, the mutated forms of Nppa and Nppb lack the C-terminal portion of the protein, which contains the mature peptides produced following processing (Fig. 1B) (Bloch

Development • Accepted manuscript

et al., 1985). Given that targeting the propeptide region of Nppa has previously been shown to result in undetectable amounts of Nppa protein (John et al., 1995), we surmise that the *nppa*^{uq19ks}, *nppb*^{uq20ks} and *nppb*^{uq21ks} alleles are functional nulls.

The incross of *nppa*$^{+/uq19ks}$ and *nppb*$^{+/uq21ks}$ single carriers generated embryos that, at the developmental stages analysed (48, 72 and 96 hours post fertilisation [hpf]), appeared wildtype, thus in line with the absence of phenotype in *Nppa*$^{-/-}$ and *Nppb*$^{-/-}$ mouse embryos as well as zebrafish single morphants (Becker et al., 2014; John et al., 1995; Tamura et al., 2000). In contrast, double homozygous *nppa* $^{uq19ks\ uq19ks}$/*nppb* $^{uq20ks/uq20ks}$ embryos displayed pericardial oedema starting at 48 hpf (Fig. 1D-H). The penetrance of the phenotype was incomplete and the expressivity variable. Approximately 20% of double mutants presented a wildtype phenotype and, in the remaining 80% of the genotypically mutant embryos, pericardial oedema was accompanied by additional cardiac abnormalities, such as looping defects, blood regurgitation at the inflow tract or both (Fig. 1H; Movie 1). One day later, the penetrance increased (Fig. 1H). These data confirm that Nppa and Nppb do indeed function redundantly and play a role during vertebrate cardiac development.

To establish whether compensation at the level of gene expression exists between *nppa* and *nppb*, we performed ISH expression analysis on both single and double mutant embryos (Fig. 1C, Fig. S1). The intensity of both *nppa* or *nppb* staining was unaltered at all stages and genotypes analysed, with the exception of *nppb* (Fig. 1C and Fig. S1). To quantify the expression of *nppa* and *nppb* levels to address the question of compensation, we performed Q-PCR analysis on single *nppa* and *nppb* mutant embryos compared with wildtype sibling controls. No significant difference was observed for any groups tested (Fig. S1). This demonstrates that there is no compensation occurring for these genes and is consistent with reports that *nppa* and *nppb* are co-regulated (Becker et al., 2012; Sergeeva et al., 2016; Sergeeva et al., 2014).

Cardiomyocyte number and size and cardiac output are all unchanged in double mutants

Previous studies inhibiting *nppa* and *nppb* expression via double morpholino knockdown have described increased cardiomyocyte numbers in double morphant embryos (Becker et al., 2014). To examine whether we observe a difference in cardiomyocyte number in double mutant versus sibling embryos, we crossed double heterozygous carriers onto the

Development • Accepted manuscript

Tg(myl7:dsRed-nls) background (labeling cardiomyocyte nuclei) and quantified cell number from confocal z-stack images. In contrast to double morpholino-treated embryos, we observed no significant difference in cardiomyocyte number in double mutant embryos compared with siblings (Fig. 2A,A').

Natriuretic peptides are well-known for counteracting cardiac hypertrophy (Lerman et al., 1993; Vanderheyden et al., 2004) and, conversely, mice null for *Nppa* or the receptor shared by Nppa and Nppb, *Npr1*, display cardiac enlargement and augmented cardiomyocyte diameter (Ellmers et al., 2007; Holtwick et al., 2003; John et al., 1995). Quantifying cardiomyocyte size in double mutant hearts compared with siblings demonstrated no difference between double mutants and siblings (Fig. B,B'). Whilst this result is in contrast with that observed in *Nppa*$^{-/-}$ and *Npr1*$^{-/-}$ mice, these prior studies examine effects after months of *Nppa* deficiency (Ellmers et al., 2007; John et al., 1995). It is perhaps this chronic loss of Nppa signalling that accounts for the discrepancy between our work and previous reports.

Next, to investigate heart function of double mutants, high-speed imaging of siblings and double mutants was performed. By observing movies of siblings versus double mutants, blood flow appeared slower when examining the inflow tract of beating hearts, which would account for the pericardial oedema observed in double mutant embryos (Movie 1). However, quantitative measurements of stroke volume and ejection fraction showed no significant difference between sibling and mutant embryos (Fig. S2). These measurements rely on comparable morphology between different groups being measured. Considering the distention of the hearts observed from pericardial oedema, this is likely to have impaired measurements and may account for no functional difference detected between siblings and mutants.

AVC markers are expanded and the cardiac jelly appears thicker in double mutant embryos

Given the repressive role *Tbx2* plays on *Nppa* expression (Christoffels et al., 2004; Habets et al., 2002), we sought to investigate if a reciprocal repressive function for Nppa on AVC-restricted gene expression takes place. To examine this, we performed ISH analysis for a range of AVC markers in sibling and double mutant embryos. Interestingly, all markers tested, namely *bmp4*, *tbx2b*, *has2* and *versican*, were expanded in double mutant embryos at

Development • Accepted manuscript

72 hpf (Fig. 2C,D). To investigate whether this resulted in a concomitant increase in the number of cells transitioning to endocardial cushion (EC) identity, immunostaining for Alcama on the *Tg(fli1a:nEGFP)*^{y7} transgenic line was performed and EC cell number quantified. Surprisingly, no significant difference was observed in the number of EC cells between sibling and double mutant embryos (Fig. S3). Instead, the expansion of AVC marker gene expression appears to affect thickening of the jelly between the layers of the cardiac wall. When high-speed movies from Figure S2 and Movie 1 were examined closely, an increased endocardial-to-myocardial thickness was consistently observed in double mutant embryos. To quantify this, the area from the outer surface of the atrial myocardium to the luminal surface of the heart was measured and a significant difference observed between sibling and double mutant embryos (Fig. 2E,E').

ssNcan-GFP is a biosensor for the cardiac jelly

We recently reported a genetically encoded biosensor to detect Hyaluronic acid (HA) in the developing embryo (De Angelis et al., 2017), using a similar approach used in cultured cells (Zhang et al., 2004). This biosensor uses the HA-binding domain of the protein, Neurocan, fused to EGFP with a synthetic secretion sequence to export it extracellularly and localise it to HA. Given that HA is a major component of the cardiac jelly, we applied this tool to examine double mutant embryos. Whilst transient mRNA injection could be used for analysing early stages of zebrafish development, we found poor reproducibility by 48 hpf in the cardiac jelly. We therefore generated a stable transgenic line, *Tg(ubi:ssNcan-EGFP)*^{uq25bh}, using the *ubiquitin* (*ubi*) promoter and observed robust and reproducible localisation of EGFP in the cardiac jelly (Fig. 3 and Movie 2). To validate that ssNcan-EGPF was indeed indicative of HA localisation and not simply an accumulation of secreted protein, we generated a ubiquitously expressing secreted GFP transgenic line (*Tg(ubi:ssEGFP)* ^{uq7ks}) and found that, not only did it have different GFP localisation to *Tg(ubi:ssNcan-EGFP)*, but almost no GFP was detected in the cardiac jelly (Fig. 3 and Movie 2), substantiating the use of the *Tg(ubi:ssNcan-EGFP)* line as a biosensor for HA and the cardiac jelly.

The cardiac jelly is increased in *nppa/nppb* double mutant hearts

To measure the cardiac jelly phenotype observed in Fig. 2E, we crossed double *nppa/nppb* carriers onto the *Tg(ubi:ssNcan-EGFP)* background and took confocal z-stacks of the hearts of anaesthetised live zebrafish. An obvious expansion of the fluorescent area was observed in double mutant embryos. Quantification showed a significant increase in ssNcan-EGFP area

Development • Accepted manuscript

in the atrium but not ventricle of double mutants compared with siblings (Fig. 4A,B). Interestingly, this correlated with the region of AVC marker gene expansion: into the atrium but not the ventricle. Of note, this included the ECM-synthetic genes, *has2* and *vesican*. *In vivo* and *in vitro* models have previously demonstrated that Nppa and Nppb exert anti-fibrotic function by inhibiting TGF-β-mediated fibroblast transformation and the production of ECM proteins (Ellmers et al., 2007; Horio et al., 2003; Li et al., 2008; Tamura et al., 2000; Tsuruda et al., 2002; Wang et al., 2003). We show here, that Nppa and Nppa exert a similar effect on ECM production during cardiac development.

Existence of a regulatory loop between Nppa/Nppb, Bmp4 and Tbx2

Given the observed increase in *bmp4* expression in *nppa/nppb* double mutants and the knowledge that *has2* expression is downstream of Bmp signalling (Shirai et al., 2009), we investigated whether inhibition of Bmp signalling is sufficient to rescue the *has2* expansion in double mutants. We injected previously published *bmp4* morpholinos (Chocron et al., 2007) into a clutch of incrossed double heterozygous carriers, grew them until 72 hpf, performed *has2* ISH, imaged and categorised embryos, followed by genotyping. We observed a robust expansion of *has2* into the atrial chamber of double mutant embryos (as observed in Fig. 2). However, *bmp4* knockdown rescued the *has2* expression pattern to that of uninjected sibling controls (Fig. 4C&D).

To investigate whether the expanded cardiac jelly in double mutants was also downstream of Bmp signalling, we injected *bmp4* morpholinos into *nppa/nppb* double mutants on the *Tg(ubi:ssNcan-EGFP)* background and measured cardiac jelly area. As observed for *has2* gene expression, the increased area of cardiac jelly in the atrium was restored to that of siblings following *bmp4* knockdown. We repeated this analysis using DMH1, a chemical inhibitor of Bmp signalling and, again, observed the cardiac jelly area restored to that of siblings (Fig. S4). Together, these data suggest that *nppa/nppb* disruption results in ectopic *bmp4* transcription into the atrial chamber and resultant increase in HA synthesis and production of cardiac jelly.

These data demonstrate that Nppa and Nppb are required to repress the AVC genetic program within the atrial chamber, providing complementarity to the activity of Tbx2b in the AVC, which represses the chamber genetic program, including *Nppa* and *Nppb*. This mutually exclusive repressive activity must assist in establishing a sharp boundary between these two

Development • Accepted manuscript

tissue compartments. Presumably, these ligands perform this function via receptor-mediated signalling, although this remains to be tested. What is still unknown is how receptor-mediated signalling acts to repress *bmp4*. We show that Nppa/Nppb signalling functions to inhibit *bmp4* transcription in the chambers, repressing the Bmp>Tbx2>Has2 cascade. The most noteworthy outcome of *nppa/nppb* deficiency is increased transcription of the extracellular matrix components *versican* and overproduction of HA.

In sum, this data reveals a previously unappreciated role for Nppa & Nppb in cardiac development. Zebrafish *nppa/nppb* double mutants develop pericardial oedema as early as 48 hpf. The functional consequence of losing Nppa/Nppb is unrestricted AVC boundary establishment, resulting in ectopic production of cardiac jelly in the atrial chamber. This role for Nppa/Nppb in restricting the Bmp-Tbx2-Has2 pathway from the chamber to the AVC, places Nppa/Nppb in a regulatory loop with Tbx2, upstream of Bmp.

MATERIALS AND METHODS

Zebrafish lines & transgenesis

All zebrafish strains were maintained and animal work performed in accordance with the guidelines of the animal ethics committee at The University of Queensland, Australia. The previously published transgenic used are *Tg(myl7:dsRed–nls)* (Mably et al., 2003); *Tg(kdrl:mCherry)* (Hogan et al., 2009) and *Tg(fli1a:nEGFP)*^{y7} (Lawson and Weinstein, 2002). Generation of the *Tg(ubi:ssEGFP)* and *Tg(ubi:ssNcan-EGFP)* lines was performed by injecting 1 nl of 25ng/µl purified plasmid DNA (constructs described in (De Angelis et al., 2017)) into single cell stage embryos together with *tol2* transposase mRNA (25ng/µl). Embryos expressing EGFP mosaically were selected and raised to adulthood and screened for germline transmission to generate stable transgenic lines.

Genome editing

TALEN monomers (Table S2) for *nppa* were generated using the golden gate kit (Cermak et al., 2011), cloned into the pCS2TAL3RR and pCS2TAL3DD backbones and transcribed as previously described (Dahlem et al., 2012). CRISPR gDNA (Table S2) and coinjection with *cas9* mRNA for targeting *nppb* was performed as described (Capon et al., 2017). Fish were screened by high resolution melt analysis (HRMA) using a Viia7 Real-Time PCR System (Applied Biosystems) and F1 embryos carrying a 4 bp deletion and 10 bp insertion for *nppa* and *nppb*, respectively, were outcrossed to wildtype strain to generate an F2 population. To

Development • Accepted manuscript

generate double mutants, *nppa* homozygous fish were incrossed and *nppb* CRISPR/Cas9 RNA injected into embryos. F1 embryos identified with a 39 bp insertion for *nppb* were outcrossed to wildtype strain to generate an F2 population. Primers for HRMA and sequencing of individual mutations are listed in Table S2.

In situ hybridisation (ISH) & antibody staining and MO injections

ISH analysis was carried out as previously described (Smith et al., 2011). Immunohistochemistry was performed as previously described (Smith et al., 2008). Antibody details are described in Table S2. The splice-targeting *bmp4* MO was used as previously described (Chocron et al., 2007). The standard *p53* control MO from Gene Tools was used.

Q-PCR analysis

DNA was extracted from the trunk of 48 hpf individual embryos as previously described (Dahlem et al., 2012) and genotyped by PCR using primer sequences depicted in Table S1. Following amplification, digestion with BsrGI-HF which cuts the wildtype sequence, was performed and successful digest resolved by agarose gel electrophoresis. *nppb* embryos were genotyped by PCR using primer sequences from Table S1, which amplify wildtype and mutant amplicons (10bp or 39bp insertion) resolved by electrophoresis on a 2.5% sodium boric acid gel (Brody and Kern, 2004) at 200 volts.

RNA was subsequently extracted from the remaining head/heart from a pool of 4 mutants or wildtype siblings in triplicate using a Direct-zol kit (Zymol Research) as per manufacturer's guidelines. qPCR for *nppa* and *nppb* was performed on a Viia 7 system (Applied Biosystems). Efficiency corrected data was normalized to the geometric average of *ef1α* and *rpl13* using GeNorm (Vandesompele et al., 2002) as previously described (Coxam et al., 2014).

Development • Accepted manuscript

DMH1 inhibitor treatment

DMH1 was dissolved in DMSO and DMSO control and DMH1 in DMSO vehicle was diluted with E3 medium to a concentration of 1μM. Embryos were dechorionated and incubated in either DMSO or DMH1 solutions for 24 hours (from 48-72 hpf), their hearts stopped with Tricaine and live imaging performed.

Live and fixed tissue imaging

Whole-mount ISH embryos were imaged using an Olympus BX51 Upright Microscope Stand with Olympus DP70 CCD camera (10× dry objective). Confocal imaging was performed on a Zeiss Axiovert 200 Inverted Microscope Stand with LSM 710 Meta Confocal Scanner using 20× and 40× dry objectives (Zeiss Zen 2012 Black Software). High-speed movies (100fps) were acquired using a Nikon Ti-E Inverted Stand with Hamamatsu Flash 4.0 sCMOS camera (20× dry objective - NIS Elements 4.3 Software). Fixed and live embryos for confocal imaging as well as live embryos for movie acquisition were mounted in low-melting 1% agarose (Sigma-Aldrich).

Assessment of wall thickness and HA staining extent

Wall thickness was measured from movie acquisitions. Files were opened with the ImageJ 2.0.0 Software and individual frames analysed. The inner surface (IS) of the heart (as delimited by the endocardium) was subtracted from the myocardium-lined, outer surface, in order to obtain the overall cardiac wall area. This value was normalized against the overall perimeter, calculated as the arithmetic mean of inner and outer perimeters. For each embryo, the corresponding wall thickness was obtained by averaging the measurements of 3 consecutive beating events. The extent of HA staining in the atrium was measured from confocal acquisitions of *Tg(ubi:ssNcan-EGFP)* embryos, calculating the ratio of EGFP-labelled area out of the total chamber area. For each embryo, the final value was the average of 3 measurements on subsequent optical sections, chosen to be at the level of the atrioventricular canal (AVC) and inflow tract. As for the quantification of HA in the ventricle

Development • Accepted manuscript

(see Fig. 4A,B), relevant sections were selected to allow as clear visualisation of the chamber inner and outer outlines as possible, preferably at the level of the AVC.

Image and statistical analyses

Image analysis and quantification was performed using Fiji (ImageJ 2.0.0 Software). Measurements of cell size were conducted as previously described (Auman et al., 2007). All cellular measurements were performed on three cells per condition from at least three different embryos. Movie analyses to determine "stroke volume" and "ejection fraction" were performed as described (Bagatto and Burggren, 2006). For statistical analysis, Gaussian distribution of the data and equal variance among groups was assumed although not formally tested. The unpaired, two-tailed Student's *t*-test, or two-way ANOVA followed by Tukey's *post hoc* test for multiple comparisons was employed (Prism 7.0a Software), as reported in figure legends.

ACKNOWLEDGEMENTS

The *bmp4* morpholino was a kind gift from Jeroen Bakkers. Confocal microscopy was performed at the Australian Cancer Research Foundation's Cancer Ultrastructure and Function Facility at the IMB. The Alcama antibody (zn-8) was obtained from the Developmental Studies Hybridoma Bank, created by the NICHD of the NIH and maintained at The University of Iowa, Department of Biology, Iowa City, IA 52242.

COMPETING INTERESTS

No competing interests declared.

FUNDING

D.R.G was supported by a University of Queensland (UQ) International scholarship. A.K.L was supported by a UQ Postdoctoral Fellowship. BMH was supported by a National Heart Foundation/National Health Medical Research Centre (NHMRC) Career Development Fellowship (1083811). K.A.S was part funded by an Australian Research Council (ARC) Future Fellowship (FT110100496). The research was part funded by an NHMRC project grant (GNT1123456).

Development • Accepted manuscript

REFERENCES

Auman, H.J., Coleman, H., Riley, H.E., Olale, F., Tsai, H.J., Yelon, D., 2007. Functional modulation of cardiac form through regionally confined cell shape changes. PLoS Biol 5, e53.

Bagatto, B., Burggren, W., 2006. A three-dimensional functional assessment of heart and vessel development in the larva of the zebrafish (Danio rerio). Physiol Biochem Zool 79, 194-201.

Becker, J.R., Chatterjee, S., Robinson, T.Y., Bennett, J.S., Panakova, D., Galindo, C.L., Zhong, L., Shin, J.T., Coy, S.M., Kelly, A.E., Roden, D.M., Lim, C.C., MacRae, C.A., 2014. Differential activation of natriuretic peptide receptors modulates cardiomyocyte proliferation during development. Development 141, 335-345.

Becker, J.R., Robinson, T.Y., Sachidanandan, C., Kelly, A.E., Coy, S., Peterson, R.T., MacRae, C.A., 2012. In vivo natriuretic peptide reporter assay identifies chemical modifiers of hypertrophic cardiomyopathy signalling. Cardiovasc Res 93, 463-470.

Bloch, K.D., Scott, J.A., Zisfein, J.B., Fallon, J.T., Margolies, M.N., Seidman, C.E., Matsueda, G.R., Homcy, C.J., Graham, R.M., Seidman, J.G., 1985. Biosynthesis and secretion of proatrial natriuretic factor by cultured rat cardiocytes. Science 230, 1168-1171.

Brody, J.R., Kern, S.E., 2004. Sodium boric acid: a Tris-free, cooler conductive medium for DNA electrophoresis. Biotechniques 36, 214-216.

Camenisch, T.D., Spicer, A.P., Brehm-Gibson, T., Biesterfeldt, J., Augustine, M.L., Calabro, A., Jr., Kubalak, S., Klewer, S.E., McDonald, J.A., 2000. Disruption of hyaluronan synthase-2 abrogates normal cardiac morphogenesis and hyaluronan-mediated transformation of epithelium to mesenchyme. J Clin Invest 106, 349-360.

Capon, S.J., Baillie, G.J., Bower, N.I., da Silva, J.A., Paterson, S., Hogan, B.M., Simons, C., Smith, K.A., 2017. Utilising polymorphisms to achieve allele-specific genome editing in zebrafish. Biol Open 6, 125-131.

Cermak, T., Doyle, E.L., Christian, M., Wang, L., Zhang, Y., Schmidt, C., Baller, J.A., Somia, N.V., Bogdanove, A.J., Voytas, D.F., 2011. Efficient design and assembly of custom TALEN and other TAL effector-based constructs for DNA targeting. Nucleic Acids Res 39, e82.

Chi, N.C., Shaw, R.M., De Val, S., Kang, G., Jan, L.Y., Black, B.L., Stainier, D.Y., 2008. Foxn4 directly regulates tbx2b expression and atrioventricular canal formation. Genes Dev 22, 734-739.

Chocron, S., Verhoeven, M.C., Rentzsch, F., Hammerschmidt, M., Bakkers, J., 2007. Zebrafish Bmp4 regulates left-right asymmetry at two distinct developmental time points. Dev Biol 305, 577-588.

Development • Accepted manuscript

Christoffels, V.M., Hoogaars, W.M., Tessari, A., Clout, D.E., Moorman, A.F., Campione, M., 2004. T-box transcription factor Tbx2 represses differentiation and formation of the cardiac chambers. Dev Dyn 229, 763-770.

Coxam, B., Sabine, A., Bower, N.I., Smith, K.A., Pichol-Thievend, C., Skoczylas, R., Astin, J.W., Frampton, E., Jaquet, M., Crosier, P.S., Parton, R.G., Harvey, N.L., Petrova, T.V., Schulte-Merker, S., Francois, M., Hogan, B.M., 2014. Pkd1 regulates lymphatic vascular morphogenesis during development. Cell Rep 7, 623-633.

Dahlem, T.J., Hoshijima, K., Jurynec, M.J., Gunther, D., Starker, C.G., Locke, A.S., Weis, A.M., Voytas, D.F., Grunwald, D.J., 2012. Simple methods for generating and detecting locus-specific mutations induced with TALENs in the zebrafish genome. PLoS Genet 8, e1002861.

De Angelis, J.E., Lagendijk, A.K., Chen, H., Tromp, A., Bower, N.I., Tunny, K.A., Brooks, A.J., Bakkers, J., Francois, M., Yap, A.S., Simons, C., Wicking, C., Hogan, B.M., Smith, K.A., 2017. Tmem2 Regulates Embryonic Vegf Signaling by Controlling Hyaluronic Acid Turnover. Dev Cell 40, 123-136.

Ellmers, L.J., Scott, N.J., Piuhola, J., Maeda, N., Smithies, O., Frampton, C.M., Richards, A.M., Cameron, V.A., 2007. Npr1-regulated gene pathways contributing to cardiac hypertrophy and fibrosis. J Mol Endocrinol 38, 245-257.

Habets, P.E., Moorman, A.F., Clout, D.E., van Roon, M.A., Lingbeek, M., van Lohuizen, M., Campione, M., Christoffels, V.M., 2002. Cooperative action of Tbx2 and Nkx2.5 inhibits ANF expression in the atrioventricular canal: implications for cardiac chamber formation. Genes Dev 16, 1234-1246.

Harrelson, Z., Kelly, R.G., Goldin, S.N., Gibson-Brown, J.J., Bollag, R.J., Silver, L.M., Papaioannou, V.E., 2004. Tbx2 is essential for patterning the atrioventricular canal and for morphogenesis of the outflow tract during heart development. Development 131, 5041-5052.

Hogan, B.M., Bos, F.L., Bussmann, J., Witte, M., Chi, N.C., Duckers, H.J., Schulte-Merker, S., 2009. Ccbe1 is required for embryonic lymphangiogenesis and venous sprouting. Nat Genet 41, 396-398.

Holtwick, R., van Eickels, M., Skryabin, B.V., Baba, H.A., Bubikat, A., Begrow, F., Schneider, M.D., Garbers, D.L., Kuhn, M., 2003. Pressure-independent cardiac hypertrophy in mice with cardiomyocyte-restricted inactivation of the atrial natriuretic peptide receptor guanylyl cyclase-A. J Clin Invest 111, 1399-1407.

Horio, T., Tokudome, T., Maki, T., Yoshihara, F., Suga, S., Nishikimi, T., Kojima, M., Kawano, Y., Kangawa, K., 2003. Gene expression, secretion, and autocrine action of C-type natriuretic peptide in cultured adult rat cardiac fibroblasts. Endocrinology 144, 2279-2284.

Development • Accepted manuscript

Inoue, K., Naruse, K., Yamagami, S., Mitani, H., Suzuki, N., Takei, Y., 2003. Four functionally distinct C-type natriuretic peptides found in fish reveal evolutionary history of the natriuretic peptide system. Proc Natl Acad Sci U S A 100, 10079-10084.

John, S.W., Krege, J.H., Oliver, P.M., Hagaman, J.R., Hodgin, J.B., Pang, S.C., Flynn, T.G., Smithies, O., 1995. Genetic decreases in atrial natriuretic peptide and salt-sensitive hypertension. Science 267, 679-681.

Keyes, W.M., Logan, C., Parker, E., Sanders, E.J., 2003. Expression and function of bone morphogenetic proteins in the development of the embryonic endocardial cushions. Anat Embryol (Berl) 207, 135-147.

Lawson, N.D., Weinstein, B.M., 2002. In vivo imaging of embryonic vascular development using transgenic zebrafish. Dev Biol 248, 307-318.

Lerman, A., Gibbons, R.J., Rodeheffer, R.J., Bailey, K.R., McKinley, L.J., Heublein, D.M., Burnett, J.C., Jr., 1993. Circulating N-terminal atrial natriuretic peptide as a marker for symptomless left-ventricular dysfunction. Lancet 341, 1105-1109.

Li, P., Wang, D., Lucas, J., Oparil, S., Xing, D., Cao, X., Novak, L., Renfrow, M.B., Chen, Y.F., 2008. Atrial natriuretic peptide inhibits transforming growth factor beta-induced Smad signaling and myofibroblast transformation in mouse cardiac fibroblasts. Circ Res 102, 185-192.

Ma, L., Lu, M.F., Schwartz, R.J., Martin, J.F., 2005. Bmp2 is essential for cardiac cushion epithelial-mesenchymal transition and myocardial patterning. Development 132, 5601-5611.

Mably, J.D., Mohideen, M.A., Burns, C.G., Chen, J.N., Fishman, M.C., 2003. heart of glass regulates the concentric growth of the heart in zebrafish. Curr Biol 13, 2138-2147.

Sergeeva, I.A., Hooijkaas, I.B., Ruijter, J.M., van der Made, I., de Groot, N.E., van de Werken, H.J., Creemers, E.E., Christoffels, V.M., 2016. Identification of a regulatory domain controlling the Nppa-Nppb gene cluster during heart development and stress. Development 143, 2135-2146.

Sergeeva, I.A., Hooijkaas, I.B., Van Der Made, I., Jong, W.M., Creemers, E.E., Christoffels, V.M., 2014. A transgenic mouse model for the simultaneous monitoring of ANF and BNP gene activity during heart development and disease. Cardiovasc Res 101, 78-86.

Shirai, M., Imanaka-Yoshida, K., Schneider, M.D., Schwartz, R.J., Morisaki, T., 2009. T-box 2, a mediator of Bmp-Smad signaling, induced hyaluronan synthase 2 and Tgfbeta2 expression and endocardial cushion formation. Proc Natl Acad Sci U S A 106, 18604-18609.

Smith, K.A., Chocron, S., von der Hardt, S., de Pater, E., Soufan, A., Bussmann, J., Schulte-Merker, S., Hammerschmidt, M., Bakkers, J., 2008. Rotation and asymmetric development of the zebrafish heart requires directed migration of cardiac progenitor cells. Dev Cell 14, 287-297.

Development • Accepted manuscript

Smith, K.A., Lagendijk, A.K., Courtney, A.D., Chen, H., Paterson, S., Hogan, B.M., Wicking, C., Bakkers, J., 2011. Transmembrane protein 2 (Tmem2) is required to regionally restrict atrioventricular canal boundary and endocardial cushion development. Development 138, 4193-4198.

Tamura, N., Ogawa, Y., Chusho, H., Nakamura, K., Nakao, K., Suda, M., Kasahara, M., Hashimoto, R., Katsuura, G., Mukoyama, M., Itoh, H., Saito, Y., Tanaka, I., Otani, H., Katsuki, M., 2000. Cardiac fibrosis in mice lacking brain natriuretic peptide. Proc Natl Acad Sci U S A 97, 4239-4244.

Tamura, N., Ogawa, Y., Yasoda, A., Itoh, H., Saito, Y., Nakao, K., 1996. Two cardiac natriuretic peptide genes (atrial natriuretic peptide and brain natriuretic peptide) are organized in tandem in the mouse and human genomes. J Mol Cell Cardiol 28, 1811-1815.

Tien, J.Y., Spicer, A.P., 2005. Three vertebrate hyaluronan synthases are expressed during mouse development in distinct spatial and temporal patterns. Dev Dyn 233, 130-141.

Tsuruda, T., Boerrigter, G., Huntley, B.K., Noser, J.A., Cataliotti, A., Costello-Boerrigter, L.C., Chen, H.H., Burnett, J.C., Jr., 2002. Brain natriuretic Peptide is produced in cardiac fibroblasts and induces matrix metalloproteinases. Circ Res 91, 1127-1134.

Vanderheyden, M., Goethals, M., Verstreken, S., De Bruyne, B., Muller, K., Van Schuerbeeck, E., Bartunek, J., 2004. Wall stress modulates brain natriuretic peptide production in pressure overload cardiomyopathy. J Am Coll Cardiol 44, 2349-2354.

Vandesompele, J., De Preter, K., Pattyn, F., Poppe, B., Van Roy, N., De Paepe, A., Speleman, F., 2002. Accurate normalization of real-time quantitative RT-PCR data by geometric averaging of multiple internal control genes. Genome Biol 3, RESEARCH0034.

Verhoeven, M.C., Haase, C., Christoffels, V.M., Weidinger, G., Bakkers, J., 2011. Wnt signaling regulates atrioventricular canal formation upstream of BMP and Tbx2. Birth Defects Res A Clin Mol Teratol 91, 435-440.

Walsh, E.C., Stainier, D.Y., 2001. UDP-glucose dehydrogenase required for cardiac valve formation in zebrafish. Science 293, 1670-1673.

Wang, D., Oparil, S., Feng, J.A., Li, P., Perry, G., Chen, L.B., Dai, M., John, S.W., Chen, Y.F., 2003. Effects of pressure overload on extracellular matrix expression in the heart of the atrial natriuretic peptide-null mouse. Hypertension 42, 88-95.

Zhang, H., Baader, S.L., Sixt, M., Kappler, J., Rauch, U., 2004. Neurocan-GFP fusion protein: a new approach to detect hyaluronan on tissue sections and living cells. J Histochem Cytochem 52, 915-922.

Development • Accepted manuscript

Figures

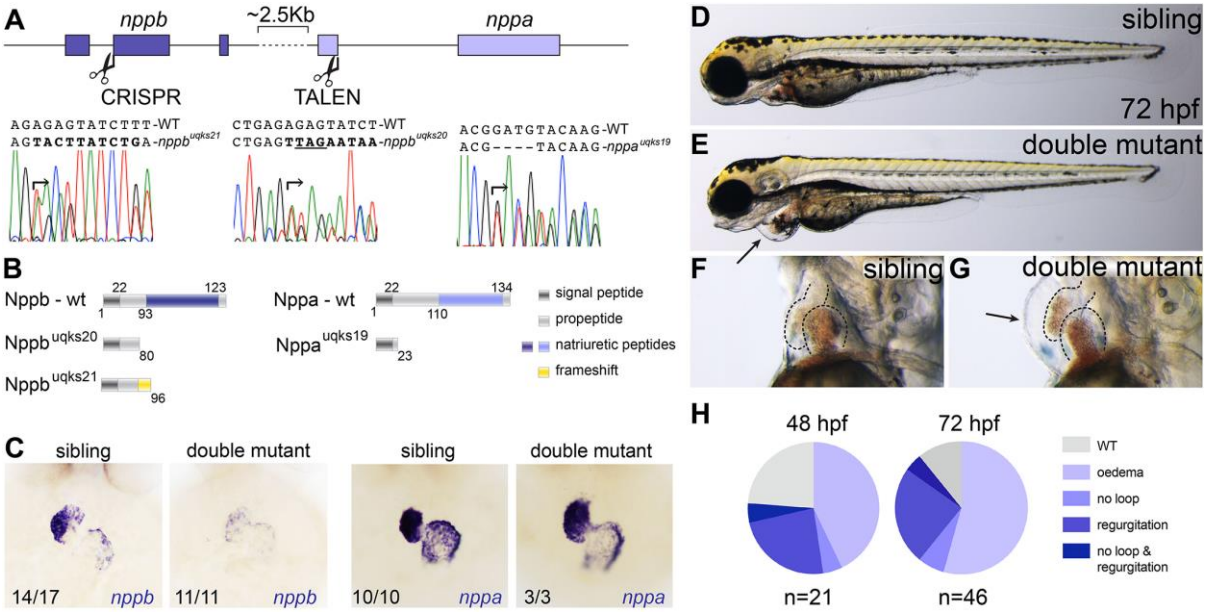

Fig. 1. Nppa and Nppb play redundant roles during early cardiac development. A. Schematic of the zebrafish *nppb* and *nppa* gene cluster (on chromosome 8) and respective *nppb* CRISPR/Cas9 (base pair 239) and *nppa* TALEN cleavage sites (base pair 54). Sanger sequencing show three alleles of *nppa* and *nppb* genes identified following genome-editing (*nppa*^{uq19ks}, *nppb* ^{uq20ks} and *nppb* ^{uq21ks}, respectively). **B.** Schematics of Nppa and Nppb wildtype and mutant proteins. Numbers indicate predicted amino acid positions. **C.** ISH for *nppa* and *nppb* on sibling and double mutant embryos at 48 hpf demonstrate overtly wildtype morphology of double mutant hearts. *nppa* gene expression is unaltered in double mutants whereas *nppb* appears decreased in double mutants. **D-G.** Lateral brightfield images of representative 72 hours post fertilization (hpf) sibling and double mutant embryos. Black arrow indicates pericardial oedema observed in double mutants. **H.** Pie charts illustrate the penetrance and expressivity of the phenotype at 48 hpf and 72 hpf.

Development • Accepted manuscript

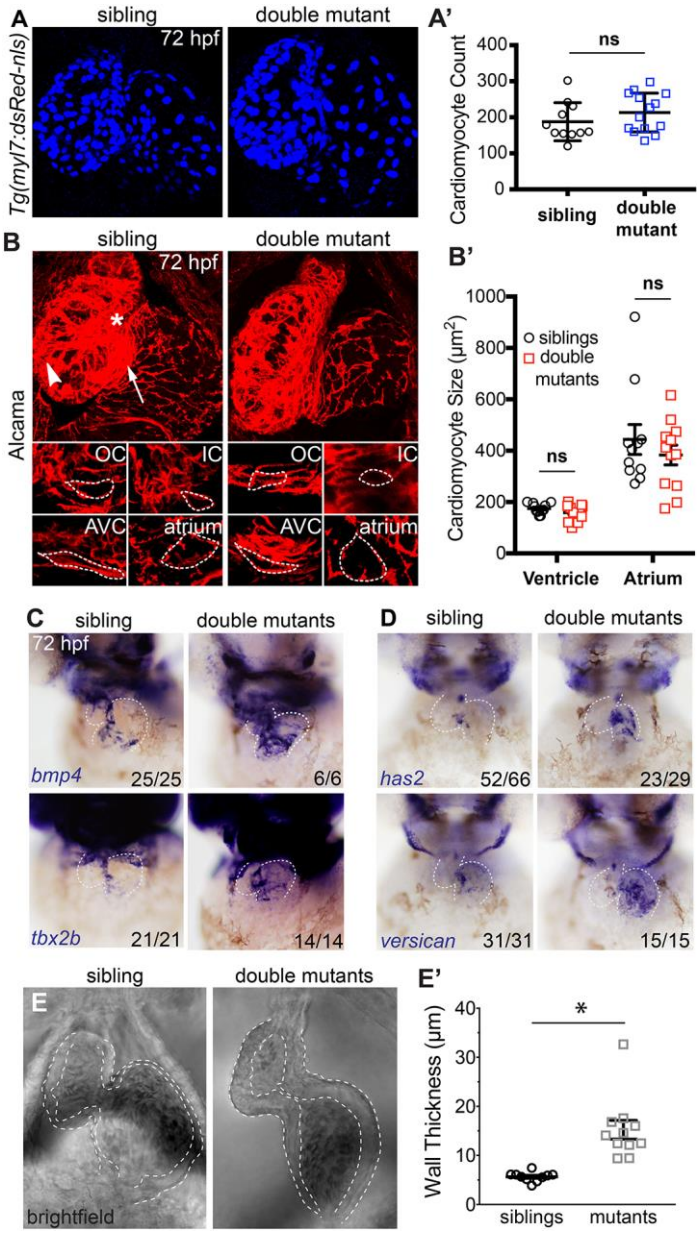

Fig. 2. AVC markers are expanded in double mutant embryos and cardiac jelly is thicker. A. Confocal z-stacks of *Tg(myl7:dsRed-nls)* embryos (labeling cardiomyocyte nuclei) show no difference in cell number between sibling and double mutant embryos. (A') Graphical representation of cell number (*n*=11 siblings; *n*=14 mutants). **B.** Confocal images of representative sibling and double mutant embryos immunostained for Alcama to visualise cell shape. IC: inner curvature [white asterisk]; OC: outer curvature [white arrowhead]; AVC: atrioventricular canal [white arrow]) (B') Graph showing average cardiomyocyte size of ventricle and atrium in siblings and double mutants (*n*=11 siblings; *n*=12 mutants). **C.** ISH analysis of AVC markers *bmp4*, *tbx2b*, *has2* and *versican* are expanded into the atrial chamber of double mutants compared with siblings. **E.** Brightfield still images from high-

Development • Accepted manuscript

speed movies of hearts at atrial diastole show thickened space between the myocardial outer surface and the lumen surface of the heart, indicating thicker cardiac jelly in double mutants. **E'.** Quantification of cardiac jelly thickness showing a significant increase in double mutant embryos compared with siblings when measuring the outer atrial myocardial wall and the inner luminal lining (*n*=10 siblings; *n*=11 mutants). ns = not significant, * p <0.05 as determined by t-test. Error bars depict mean+SD.

Development • Accepted manuscript

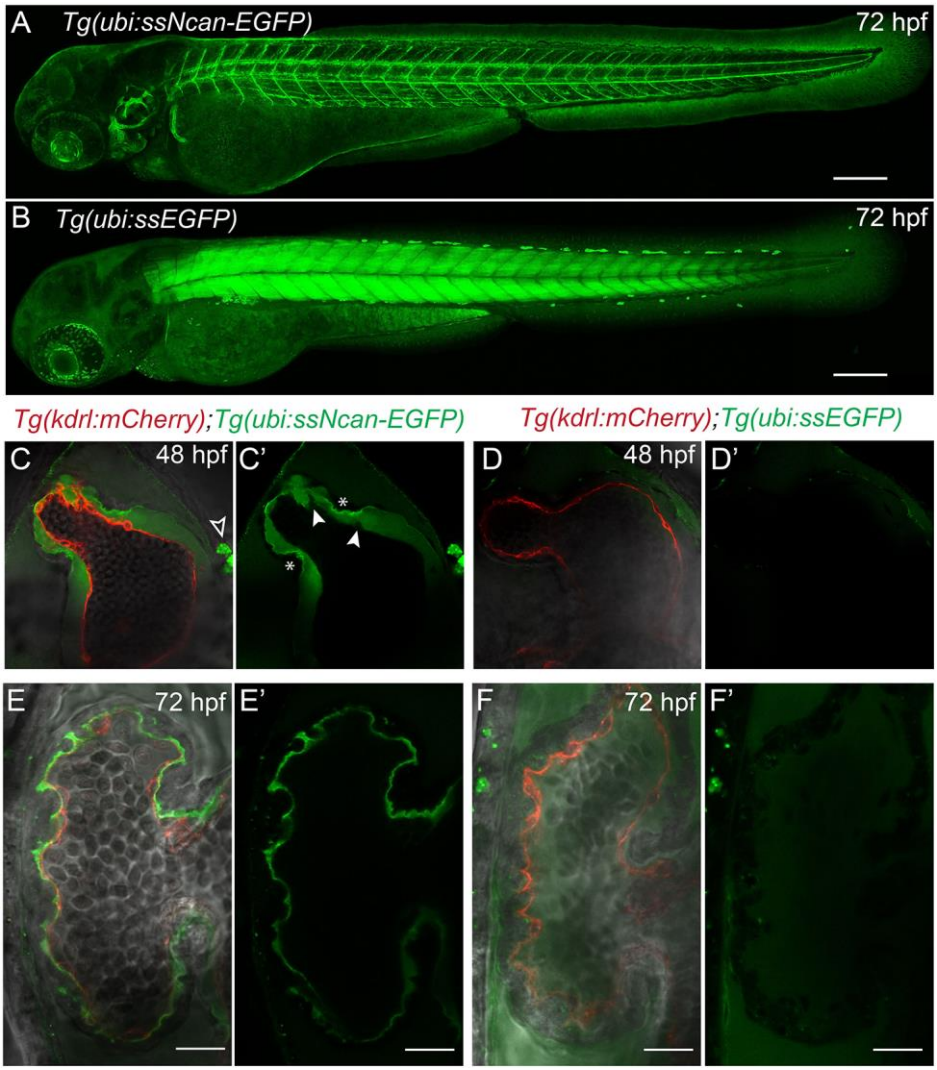

Fig. 3. A transgenic biosensor for the cardiac jelly. A. Lateral view of the *Tg(ubi:ssNcan-EGFP)* line: a biosensor for Hyaluronic acid - a major constituent of the cardiac jelly. The sensor expresses a secreted fusion protein of the HA-binding domain of Neurocan fused to GFP, driven by the *ubi* promoter. The biosensor localizes to regions of HA, including the cardiac jelly, the otic vesicle and around the vasculature. **B.** The *Tg(ubi:ssEGFP)* control was also generated and shows different EGFP localisation, predominantly to the skeletal muscle. Scale bar = 100µm. **C&C'.** Frontal view images of 48 hpf *Tg(ubi:ssNcan-EGFP)*/*Tg(kdrl:mCherry)* hearts anaesthetized and live-imaged showing the cardiac jelly (green) and endocardial layer (red). ssNcan-EGFP localizes to mucus cells (black arrowhead) and is concentrated at the AVC (asterisks). Regions devoid of ssNcan-EGFP in the cardiac jelly due to protruding endocardial cells can also be observed (white arrow heads). **D&D'**. Live images of 48 hpf *Tg(ubi:ssEGFP)*/*Tg(kdrl:mCherry)* hearts showing near undetectable amounts of ssEGFP localization (for full z-stacks of C&D - see Movie 2). **E&E'.** Live

Development • Accepted manuscript

images of 72 hpf *Tg(ubi:ssNcan-EGFP)*/*Tg(kdrl:mCherry)* ventricles showing condensed jelly and sites of trabeculae formation. **F&F'.** Live images of 72 hpf *Tg(ubi:ssEGFP)*/*Tg(kdrl:mCherry)* hearts showing ssEGFP localization in the pericardial space. Scale bar = 20µm.

Development • Accepted manuscript

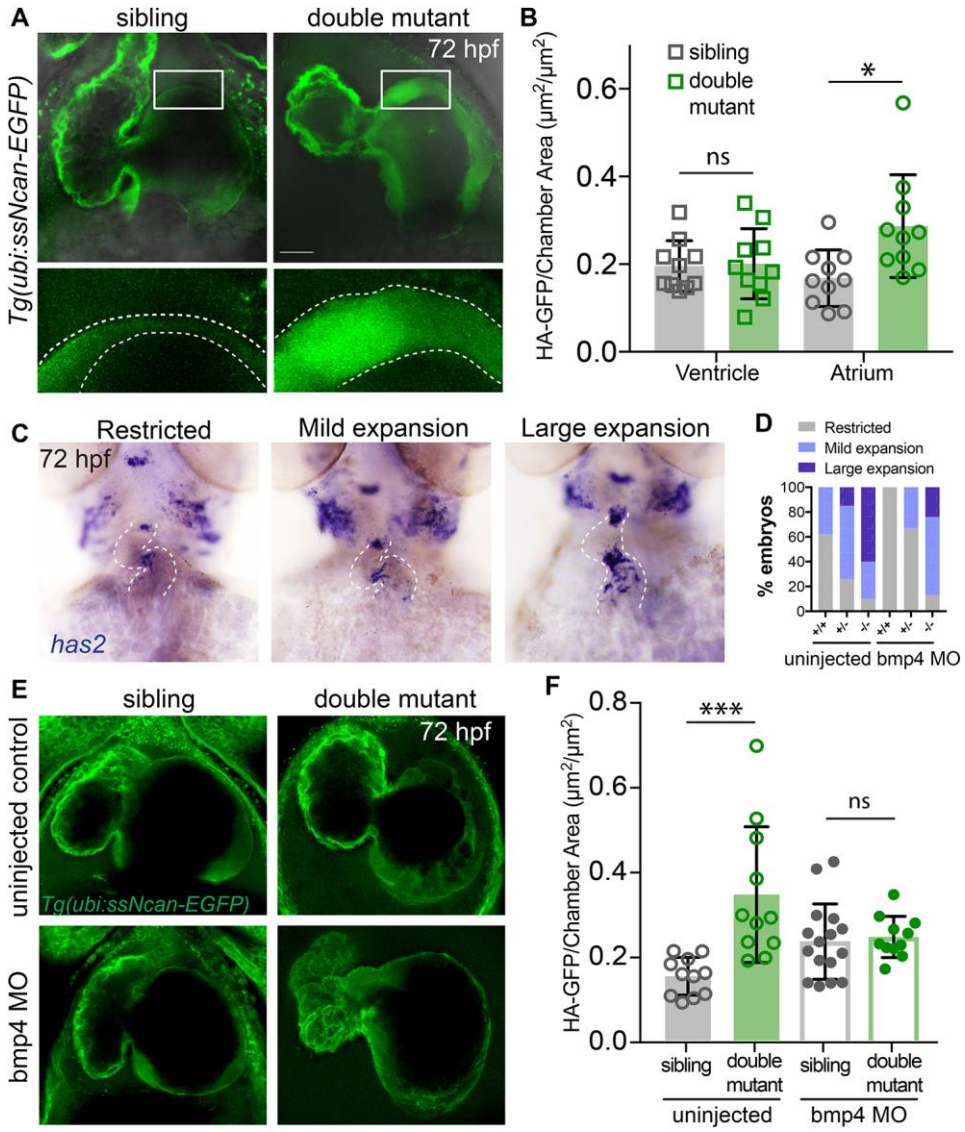

Fig. 4. Cardiac jelly is increased in double mutant embryos and the AVC expansion is downstream of Bmp4 signalling. A. Representative confocal stacks of the cardiac jelly in siblings versus double mutant embryos (ventral view, head to the top), demonstrating thicker cardiac jelly in double mutant embryos at 72 hpf. **B.** Dot plot depicting the measurement of cardiac jelly area, showing no significant difference (ns) in jelly thickness of ventricles of siblings versus mutants, whereas significantly more jelly in the atrium of double mutants compared with siblings is observed (n=10; * $p < 0.05$; two-tailed t-test). Error bars indicate mean+SD. **C.** Representative images of embryos following ISH for *has2* expression in sibling and double mutant embryos. Images show categories of *has2* expression in embryos at 72 hpf. **D.** Graphical representation of the proportion of embryos with different categories of *has2* expression in wildtype (n=13), double heterozygotes (n=34) and double mutant (n=10) embryos in uninjected controls or in wildtype (n=5), double heterozygotes (n=9) and

Development • Accepted manuscript

double mutant (*n*=8) embryos following *bmp4* knockdown. The proportion of phenotypes in double mutant embryos injected with *bmp4* morpholino most closely resembles uninjected double heterozygotes, demonstrating restoration of *has2* expression upon *bmp4* knockdown. **E.** Representative confocal stacks of *Tg(ubi:ssNcan-EGFP)* to visualise the cardiac jelly in siblings versus double mutant embryos at 72 hpf, either uninjected or injected with *bmp4* morpholino. **F.** Dot plots depicting the measurement of cardiac jelly area in atria of sibling versus double mutant embryos. A significant increase in the jelly area is observed between uninjected siblings and double mutants (*n*=11; *** $p < 0.01$; two-way ANOVA for multiple comparisons with Tukey's *post hoc* correction). No significant difference (ns) is observed in the jelly area between siblings and double mutants following *bmp4* morpholino injection (*n*=16 siblings; *n*=11 double mutants), demonstrating that the increase in the cardiac jelly thickness is restored following *bmp4* morpholino injection. Two-tailed t-test, error bars indicate mean+SD.

Development • Accepted manuscript

Supplementary Data and Tables

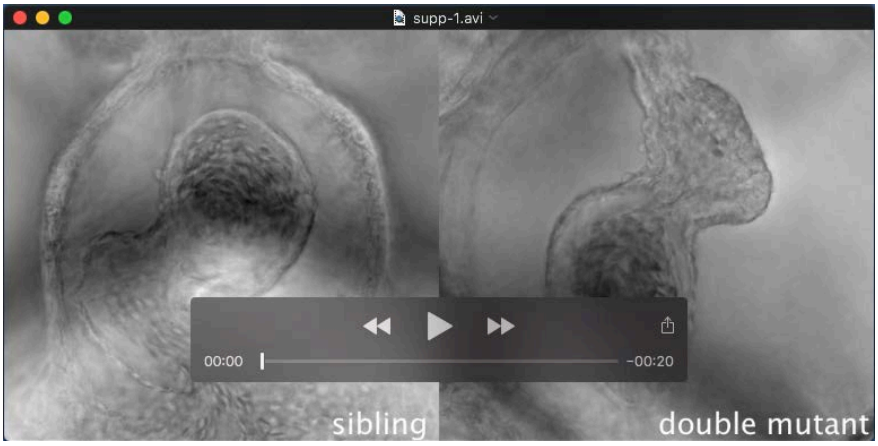

Movie 1. High-speed, brightfield movies of functioning sibling (left) and double mutant (right) hearts at 72 hpf, viewed ventrally.

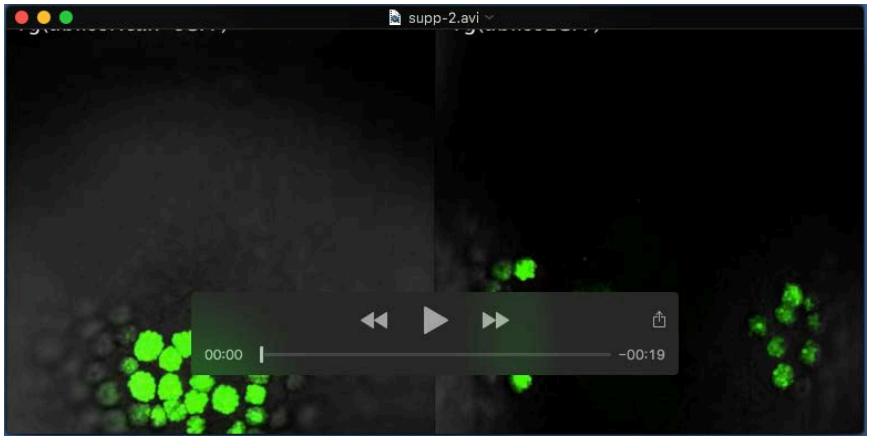

Movie 2. Z-stack series of 48 hpf hearts of *Tg(ubi:ssNcan-EGFP)*/*Tg(kdrl:mCherry)* (left) and *Tg(ubi:ssNcan-EGFP)*/*Tg(kdrl:mCherry)* (right), viewed ventrally. Partial stacks are represented in Fig. 3C&D.

Development • Supplementary information

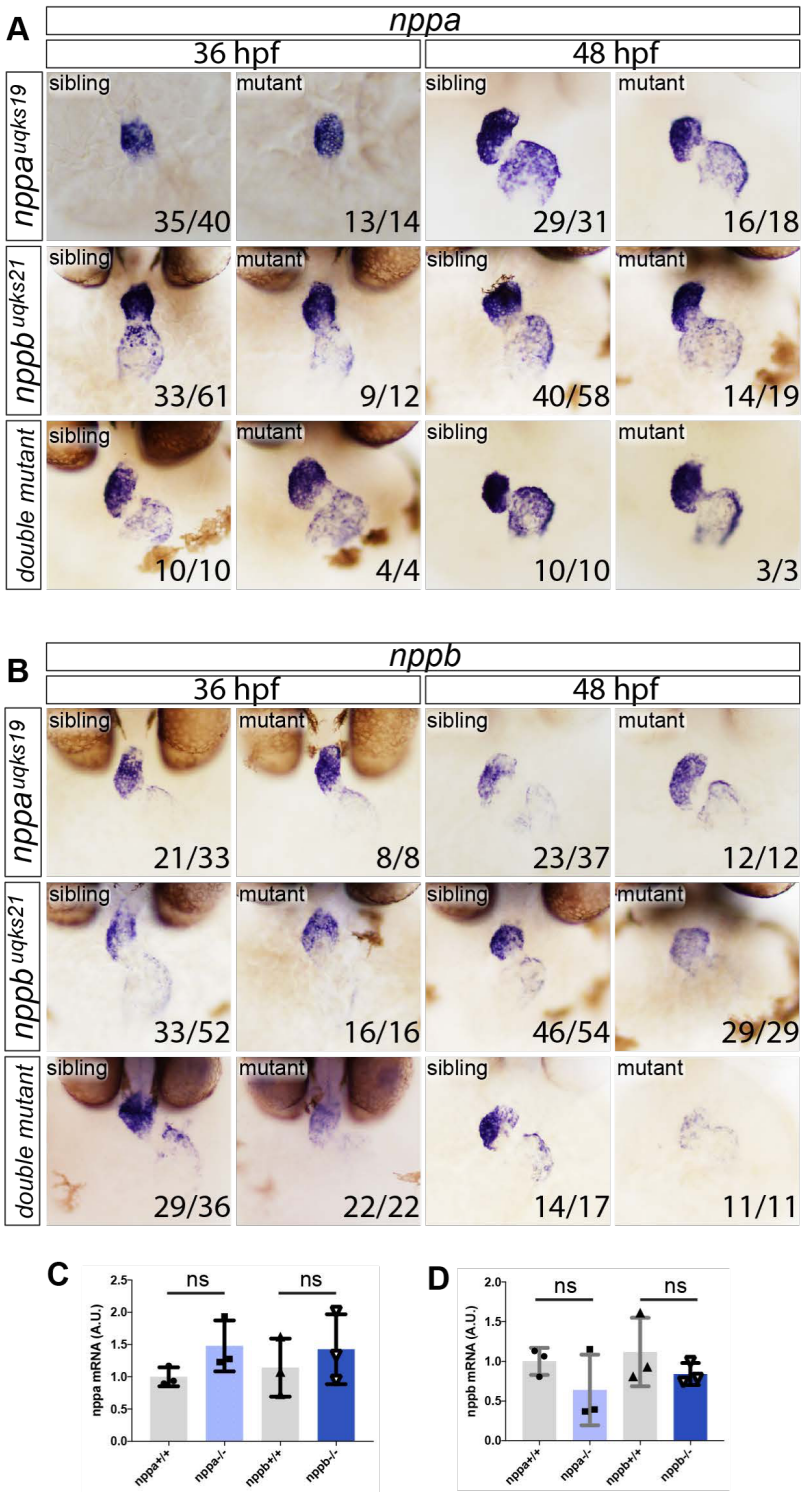

Fig. S1. ISH expression analysis of *nppa* and *nppb* in siblings, single *nppa* and *nppb* mutants and double mutants. Expanded expression analysis from that represented in Figure 1C, showing **A.** *nppa* and **B.** *nppb* expression at 36 and 48 hpf. No gross differences in either morphology or expression levels are observed for any of the scenarios, with the exception that *nppb* expression in *nppb* mutants (or double mutants) has reduced staining by ISH. **C.** Q-PCR

Development • Supplementary information

analysis of *nppa* expression levels in *nppa* single mutants compared with in-clutch sibling controls or *nppb* single mutants compared with siblings. No significant difference in expression is observed (ns). **D.** Q-PCR analysis of *nppb* expression on *nppa* and *nppb* single mutants compared with sibling controls showing no significant difference (ns) between groups. Two-tailed t-test on n=3 replicates, where each replicate contained pooled mRNA from 4 genotyped embryos.

Development • Supplementary information

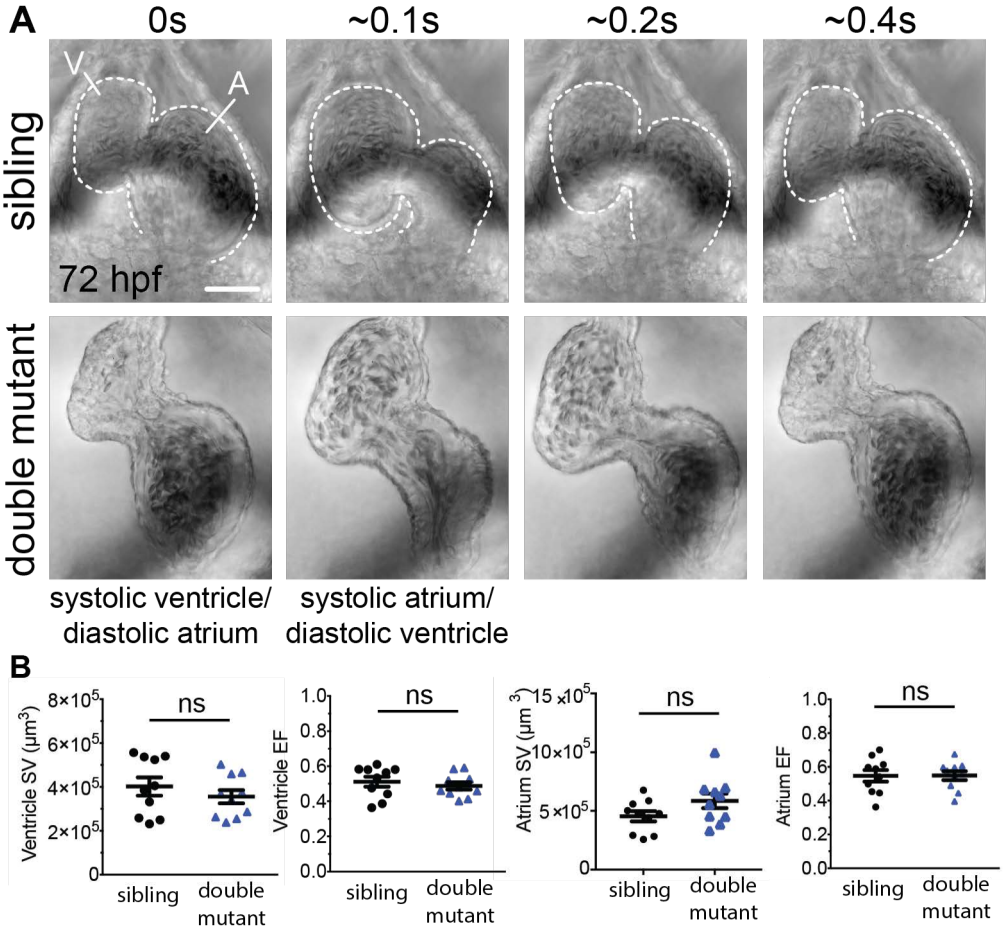

Fig. S2. Cardiac function is unchanged in *nppa/nppb* double mutants at 72 hpf. Still images from high-speed movies show phases of atrial diastole (0s), ventricular diastole/atrial systole (0.1s) and ventricular systole (0.4s). **B.** Dot plots depicting the analysis of heart function between siblings and double mutants. Ventricular stroke volume (SV), atrial stroke volume, ventricular ejection fraction (EF) and atrial ejection fraction showed no significant difference between siblings (n = 10) and double mutant embryos (n = 10). ns = not significant, two-tailed t-test, error bars indicate mean+/- s.e.m. Scale bar = 50um. V = ventricle; A = atrium.

Development • Supplementary information

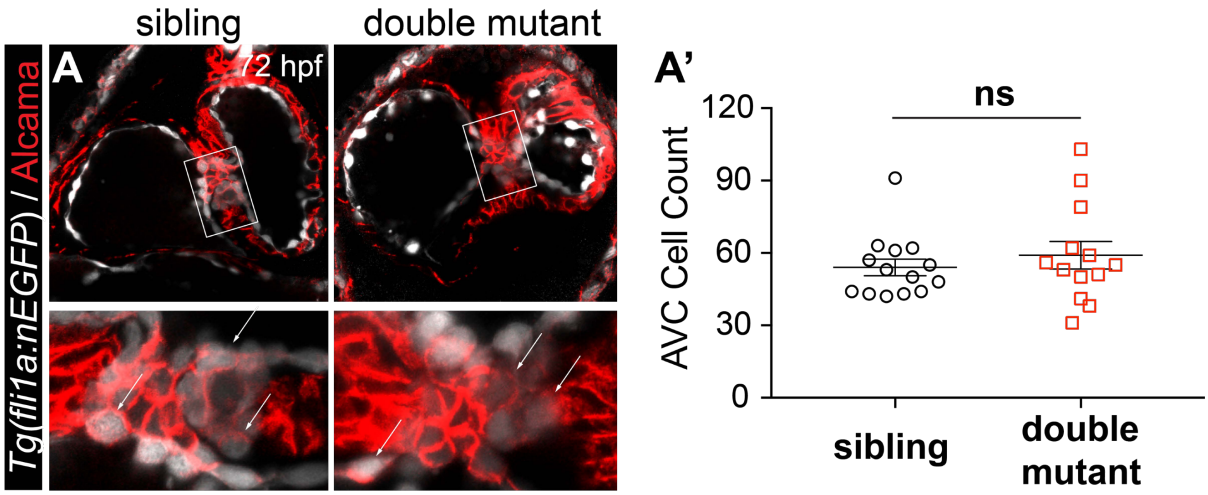

Fig. S3. No increase in endocardial cell number is observed in *nppa/nppb* double mutants compared with siblings. A. Confocal stacks of 72 hpf sibling and double mutant with endocardial nuclei labelled by *Tg(fli1a:nEGFP)* (white) and myocardial membranes labelled using an anti-Alcama antibody (red). In addition to myocardium, endocardial cushions are also labeled with Alcama, distinguishing them from the remaining endocardium. Double positive cells (white arrows) are quantified in A'. **A'.** Dot plots representing the number of AVC cells in sibling (n = 14) versus double mutants (n = 13), showing no significant difference (ns; two-tailed t-test; error bars indicate the standard error mean).

Development • Supplementary information

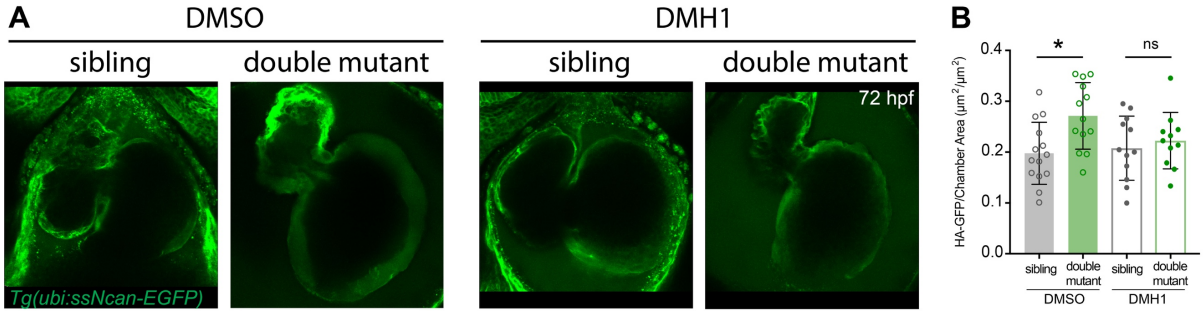

Fig. S4. A chemical inhibitor of Bmp signalling restores the area of the atrial cardiac jelly back to levels of siblings. A. Confocal stacks showing the hearts of sibling and double mutant embryos at 72 hpf in the *Tg(ubi:ssNcan-EGFP)* background treated with either DMSO control or the Bmp signalling-specific inhibitor, DMH1. Embryos were incubated for 24 hours prior to live imaging and the area of the cardiac jelly quantified for each treatment. **B.** Dot plots of cardiac jelly area for individual embryos following treatment with either DMSO or DMH1. Double mutant embryos had significantly increased cardiac jelly area compared with sibling controls; however this increase was restored to the levels of siblings, following Bmp inhibition with DMH1. DMSO siblings n=14, DMSO double mutants n=13, DMH1 siblings n=12, DMH1 double mutants n=11. Statistics was determined using a two-way ANOVA for multiple comparisons with Tukey's post hoc correction. *$p < 0.05$. ns=not significant. Error bars depict std dev.

Development • Supplementary information

Supplementary Materials & Methods

Table S1. List of oligo sequences for *nppb* probe synthesis, TALEN & CRISPR synthesis and HRMA, sequencing and Q-PCR analysis

Oligo name	**Sequence 5'-3'**
nppa TALEN forward	GCTGCTCCTGGTTTGG
nppa TALEN reverse	GCTCAACGTGTGCGCT
nppa HRMA forward	GATGGCCGGGGGACTAATTC
nppa HRMA reverse	TTGGCCATGTTGCTGTCAGA
nppb CRISPR gDNA forward	GCAGAAAGATACTCTCTC
nppb HRMA forward	GCAGCCCGATACTTACCTGA
nppb HRMA reverse	CTACCTGAGCGCCCGACT
nppa genotyping forward	AAGGAAATCTGCCCCAGCAA
nppa genotyping reverse	AGAGCACTGACTGTTTACCTC
$nppb^{uq20ks}/nppb^{uq21ks}$ sequencing forward	CACATGAGGACATTCCCGCTT
$nppb^{uq20ks}/nppb^{uq21ks}$ genotyping reverse	TGAGCGCCCGACTGTGTTAC
$nppb^{uq20ks}/nppb^{uq21ks}$ genotyping forward	GCAGCCCGATACTTACCTGA
$nppb^{uq20ks}/nppb^{uq21ks}$ sequencing reverse	CTACCTGAGCGCCCGACT
nppb probe forward	CATTCCCGTAGTCGGCCTTC
nppb probe reverse	Ggatccattaaccctcactaaagggaac CCCGACTGTGTTACATCCCAA
nppa F Q-PCR primer	ACAGCTCTGACAGCAACATGG
nppa R Q-PCR primer	CTGATGCCTCTTCTGTTGCCA
nppb F Q-PCR primer	TGTTTCGGGAGCAAACTGGA
nppb R Q-PCR primer	GTTCTTCTTGGGACCTGAGCG

Table S2. List of antibodies

Reagent name	**Dilution used**	**Source**
Mouse α-Alcama	1:500	ZN-8 (DSHB)
Rabbit α-dsRed	1:200	632496 (Living Colors)
Chicken α-GFP	1:200	AB13970 (Abcam)
Alexa 647 α-mouse	1:1000	A-21240 (Invitrogen)
Alexa 555 α-rabbit	1:1000	A-31572 (Invitrogen)
Alexa 555 α-chicken	1:1000	A-11039 (Invitrogen)

Development • Supplementary information